Received December 30, 2020; revised January 31, 2021; accepted February 7, 2021. Date of publication 10 February 2021; date of current version 1 March 2021.
The review of this article was arranged by Editor X. Guo.

Digital Object Identifier 10.1109/JEDS.2021.3058348

A Novel Real-Time TFT Threshold Voltage Compensation Method for AM-OLED Using Double Sampling of Source Node Voltage

KYEONG-SOO KANG, JIN-KYU LEE, JI-MIN KANG, AND SOO-YEON LEE

Department of Electrical and Computer Engineering, Seoul National University, Seoul 08826, South Korea

CORRESPONDING AUTHOR: S.-Y. LEE (e-mail: sooyeon.lee@snu.ac.kr)

ABSTRACT In this article, we propose a novel real-time threshold voltage (V_{th}) compensation method for AM-OLED display. The proposed method predicts V_{th} shift of driving thin-film transistors (TFTs) based on the equation derived from the sensing line charging with TFT's drain current. The prediction equation requires two consecutive source node voltages to consider the mobility variation, and only takes hundreds of microseconds to predict V_{th} shift. It is short enough to monitor the real-time V_{th} degradation, since the prediction can be carried out during the vertical blank time. Also, very high prediction accuracy was confirmed through Smart SPICE simulation. We simulated severe mobility variation and V_{th} shift circumstances, and the simulation results showed that the prediction error was less than one just noticeable difference (JND) margin though out all gray levels. We expect that the proposed method can achieve more accurate and faster real-time V_{th} degradation compensation for high resolution and large-sized OLED displays than conventional one.

INDEX TERMS OLED, threshold voltage, compensation, real-time, JND.

I. INTRODUCTION

Organic light-emitting diode (OLED) display has attracted attention due to its outstanding advantages such as wide viewing angle, high contrast ratio, and short response time [1]–[6]. In OLED display, thin-film transistors (TFTs) apply current to OLED because OLED is a current-driven device. Therefore, TFT characteristics directly affect the display image quality. Usually, TFTs suffer from process fluctuation and degradation under electrical and thermal stress during operation [7], [8], so that OLED displays require compensation for luminance non-uniformity. Several effective compensation methods have been proposed [9]–[12]. Among them, sensing and applying V_{th} to the compensation has become mainstream because TFTs' threshold voltage (V_{th}) variation is considered the major factor that affects the luminance uniformity in OLED display [12], [13].

There are two options to compensate for the degradation of V_{th}. One is internal compensation [14], [15], and the other is external compensation [16], [17]. Commercialized large-size OLED display products adopt external compensation because of its simple pixel circuit structure and high accuracy [16], [17]. This method is carried out by charging the sensing bus line's capacitive load with TFT subthreshold current. Then analog-to-digital converter in the display driver integrated circuit detects the TFT parameters. Normally external compensation method takes tens of milliseconds to detect V_{th} of each TFT [6], [13]. Therefore, real-time TFT degradation cannot be compensated during display operation. The existing method can be performed only after the display is turned off.

This article proposes a compensation method can be carried out within a vertical blank. Many studies about real-time V_{th} compensation have been conducted such as fast methods using iterative feedback [13], linear charging method [18], and current sensing [19]. However, these methods take more than the vertical blank time of the latest display products, or the non-uniform mobility is not considered. In this article, a novel real-time V_{th} degradation compensation method

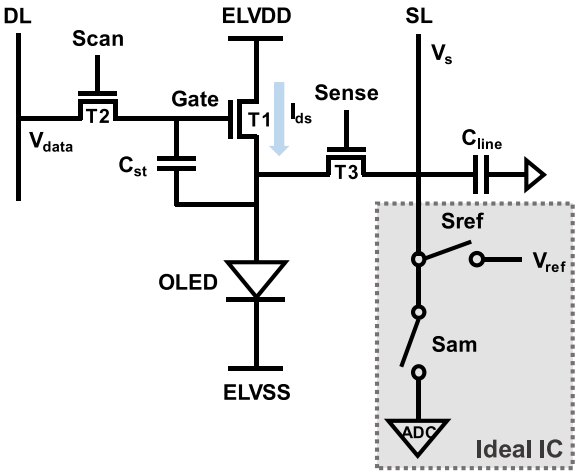

FIGURE 1. 3T1C external compensation circuit in the OLED display panel.

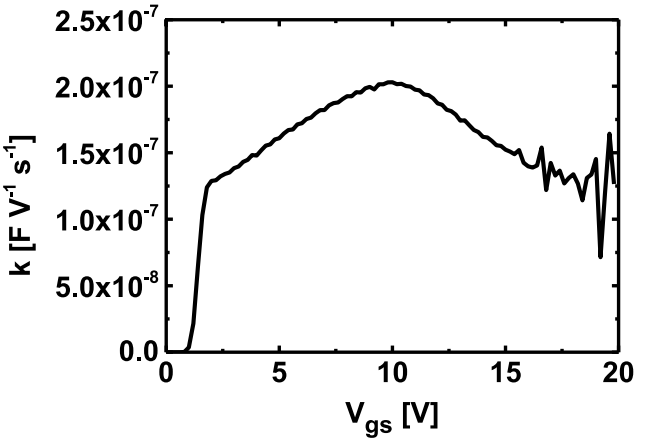

FIGURE 2. k-V_{gs} curve extracted from the measured transfer data of oxide TFT.

based on non-linear charging is proposed and verified by SPICE simulation. The proposed method takes an extremely short time to predict the V_{th} shift and only has a very small prediction error.

II. PROPOSED METHOD

The conventional external compensation circuit consists of 3 TFTs and 1 capacitor (C_{st}) [11], [20], as shown in Fig. 1. The compensation procedure is as follows. First, the Sref signal is set to high level, and the voltage of the sensing bus line (V_s) is refreshed to the initial voltage V_{ref}. Then, the Scan signal turns on T2, and the data voltage V_{data} is applied to the gate of T1. After that, the Sense signal turns on T3, and I_d charge C_{line}, the sensing line's capacitive load. T1's gate node is fixed to V_{data}, and V_s keeps increasing until the gate-to-source voltage (V_{gs}) of T1 becomes V_{th} and I_d becomes 0 A. V_{th} is detected from the difference between V_{data} and saturated V_s. These procedures take tens of milliseconds.

The proposed method is based on the V_{th} prediction equation. During V_{th} detecting, the V_{gs} of T1 is a function of time. Thus, when $V_{eff}(t) = V_{gs}(t) - V_{th}$, the drain current of T1 is expressed by,

$$I_d = k \times V_{eff}(t)^2, \tag{1}$$

$$k = \frac{1}{2}\ \mu\ C_{ox}\frac{W}{L}, \tag{2}$$

where μ is the mobility of carrier, C_{ox} is the capacitance of the gate oxide, and W/L is width/length of the device. Unlike the ideal transistor, k should be expressed as $k(V_{gs}(t))$ because mobility varies with V_{gs}. Fig. 2 shows a relationship between k and V_{gs}, which is obtained from TFT's I_d-V_{gs} measurement data through $k = (d\sqrt{I_d}/dV_{gs})^2$. For the simplicity, we established the equation with constant k first, and then the voltage dependence of k was considered.

In the aspect of C_{line}, $I_d = C_{line} \cdot dV_s(t)/dt$ is also satisfied, and $dV_s(t)/dt$ is equal to $-dV_{eff}(t)/dt$. Therefore, there is another I_d equation as follows.

$$I_d = -\ C_{line} \times \frac{dV_{eff}(t)}{dt} \tag{3}$$

According to (1) and (3), differential equation (4) is established. Using boundary condition $V_{eff}(0) = V_{gs}(0) - V_{th}$ to solve (4), $V_{eff}(t)$ equation (5) is obtained.

$$k \times V_{eff}(t)^2 = -C_{line} \times \frac{dV_{eff}(t)}{dt} \tag{4}$$

$$V_{eff}(t) = \frac{1}{\frac{1}{V_{gs}(0) - V_{th}} + \frac{k}{C_{line}}t} \tag{5}$$

Then, we can get (6) by solving (5) and $V_{eff}(t) = V_{gs}(t) - V_{th}$ for V_{th}.

$$V_{th} = V_g - \left(\frac{2\gamma}{-\beta\gamma + \sqrt{\beta^2\gamma^2 + 4\beta\gamma}} + V_s(0) \right) \tag{6}$$

$$\beta = \frac{k}{C_{line}}t\ ,\ \gamma = V_s(t) - V_s(0) \tag{7}$$

The equation in parentheses of (6) can be used as a prediction equation for saturated V_s, (8), because V_{th} is detected from the difference between V_g and saturated V_s.

$$\text{Saturated } V_s = \frac{2\gamma}{-\beta\gamma + \sqrt{\beta^2\gamma^2 + 4\beta\gamma}} + V_s(0) \tag{8}$$

As mentioned above, k should be expressed as $k(V_{gs}(t))$, or simply k(t). By approximating $I_d = C_{line} \cdot dV_s(t)/dt$ to $I_d \cdot \Delta t = C_{line} \cdot \Delta V_s(t)$ when $\Delta V_s(t) = V_s(t+\Delta t) - V_s(t)$, the equation of k(t) is obtained as (9).

$$k(t) = C_{line} \times \frac{V_s(t + \Delta t) - V_s(t)}{\Delta t} \times \frac{1}{\left(V_g - V_s(t) - V_{th}\right)^2} \tag{9}$$

Assuming $V_s(0)$ is 0 V and multiplying the denominator and numerator of (8) by $(1/\gamma)(\beta + \sqrt{\beta^2 + 4\beta/\gamma})$, the

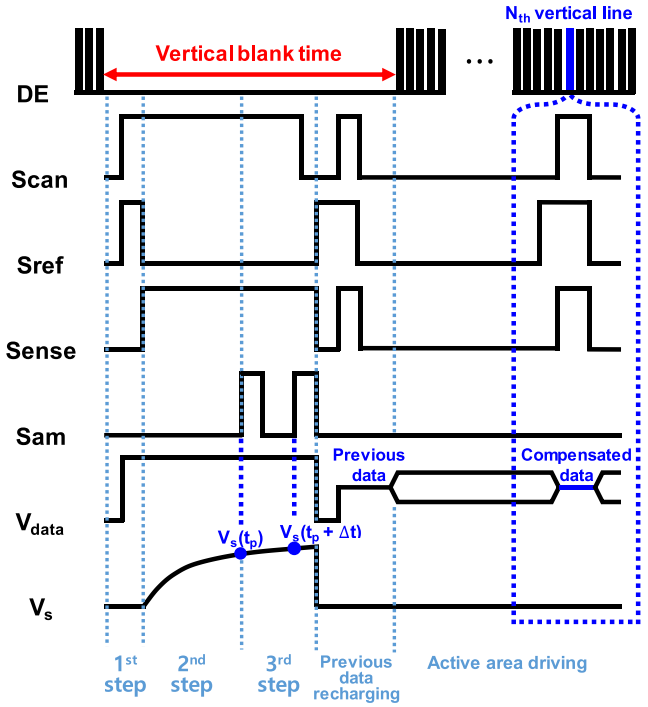

FIGURE 3. Controlling signals for the proposed circuit to calculate V_{th}.

simplified equation (10) is obtained.

$$\textbf{Saturated } V_s = \frac{\gamma}{2} + \sqrt{\frac{\gamma^2}{4} + \frac{\gamma}{\beta}} \tag{10}$$

$$\beta = \frac{k(t)}{C_{line}} t \ , \ \gamma = V_s(t) \tag{11}$$

To extract the equation for V_{th}, we subtracted $\gamma/2$ from both sides of (10) and squared them. Then, $\gamma^2/4$ is removed and (10) is expressed as (12). Since both side of (12) can be divided by $V_g - V_s(t) - V_{th}$, (12) is simplified as (13).

$$\left(V_g - V_{th}\right)^2 - V_s(t)\left(V_g - V_{th}\right) = \frac{V_s(t)}{\frac{[V_s(t+\Delta t) - V_s(t)]t}{\Delta t[V_g - V_s(t) - V_{th}]^2}} \tag{12}$$

$$V_g - V_{th} = \frac{\frac{V_s(t)^2 \Delta t}{[V_s(t+\Delta t) - V_s(t)]t}}{\frac{V_s(t)\Delta t}{[V_s(t+\Delta t) - V_s(t)]t} - 1} \tag{13}$$

Lastly, we can get the final V_{th} prediction equation (14).

$$V_{th} = V_g - \frac{V_s(t)^2 \Delta t}{V_s(t)\Delta t - [V_s(t+\Delta t) - V_s(t)]t} \tag{14}$$

Now, V_{th} is obtained from the two consecutive (t, V_s(t)) points. In other words, V_{th} can be predicted from the slight change of V_s(t). Thus, if we can extract two (t, V_s(t)) points in a short time for a short interval, we can calculate V_{th} in a short time. Fig. 3 shows the timing diagram of control signals to calculate V_{th}. The proposed method is performed in three steps during the vertical blank time.

In the first step, Scan signal and Sref signal are set to a high level when the vertical blank time is started. V_{data} is applied to the gate of T1, and V_s is refreshed to the initial voltage V_{ref}. V_{ref} is 0 V in this article. In the second step, the Sense signal is set to a high level and the Sref signal is set to a low level. The I_d flows through T3 and charges C_{line}. While C_{line} is charged, V_{gs} of T1 decreases and I_d also decreases, keeping saturation operation. OLED is kept turn-off state, since V_s is always lower than the turn-on voltage of OLED. In the third step, $V_s(t_p)$ and $V_s(t_p+\Delta t)$ is sampled at the prediction point t_p and $t_p + \Delta t$ by using Sam signal. Then, V_{th} is calculated using (14). These procedures take only hundreds of microseconds.

After the sampling, the Sref signal is set to a high level, and V_s is refreshed to 0 V. Then, the Scan signal and Sense signal are set to a high level. The previous data, equal to the voltage charged in C_{st} at the previous frame, is applied to the gate of T1 and recharges C_{st}. Therefore, a pixel under the V_s detection is interrupted during only the vertical blank time. The predicted ΔV_{th} is calculated and stored in an external IC, and then the compensated data is applied from the next refresh time.

However, V_{th} calculated from (14) is not equal to $V_{th,actual} = V_g - $(saturated V_s) in conventional external compensation. In the conventional external method, the second step continues until T1 has $I_d(V_{th})$, then V_{th} is detected. Whereas, in the proposed method, V_{th} is predicted through the ideal transistor current equation $I_d = k(V_{gs} - V_{th,predict})^2$ with early extracted voltage information. Fig. 4 shows the difference between $V_{th,actual}$ in the conventional method, and $V_{th,predict}$ in the proposed one. The black line is the measured transfer curve, and the red line represents the ideal current expression based on the extracted information. The red line fits the measured data quite well in the above-threshold region when k is extracted from (9).

However, the ideal equation does not properly reflect the current characteristic in the subthreshold region. The difference in the subthreshold region results in a difference between $V_{th,actual}$ and $V_{th,predict}$. This difference is larger than 0.3 V.

On the other hand, when it comes to ΔV_{th} instead of V_{th}, quite accurate prediction is possible. When the transfer curve changes due to V_{th} degradation, the above-threshold region projects almost the same V_{th} shift. Thus, if we compare the change of calculated V_{th} before and after the degradation, the degree of change is approximately equal to the degradation of actual V_{th}.

Table 1 shows the Smart SPICE simulation results when the oxide TFT model based on the measured transfer data is used and V_g is set to 5 V. The prediction error of ΔV_{th} is only about 0.2 mV, when prediction point is 300 μs and $\Delta V_{th,actual}$ is 10 mV. Therefore, we focus on the prediction of V_{th} shift, not the prediction of V_{th} itself in this article.

However, both V_{th} degradation and the initial V_{th} non-uniformity must be considered to obtain the compensation voltage. Thus, the initial non-uniformity of V_{th} itself should be measured using the conventional method. In other words,

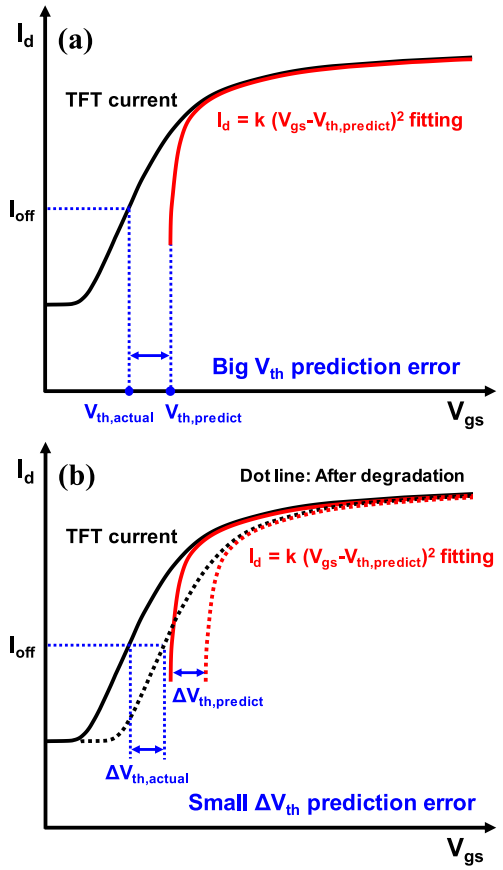

FIGURE 4. Measured transfer curve and ideally fitted curve of TFT. (a) V_{th} prediction error is big because the subthreshold slope is different. (b) ΔV_{th} prediction error is small because the change of calculated V_{th} is almost same as the actual V_{th} degradation.

TABLE 1. V_S at 300 μs from spice simulation and $V_{th,predict}$, $\Delta V_{th,predict}$.

	Before degradation	After degradation
	$V_{th,actual}$=0.69781 V	$V_{th,actual}$=0.68781 V
V_s(300 μs)	2.64572 V	2.65463 V
V_s(310 μs)	2.67468 V	2.68364 V
$V_{th,predict}$ at 300 μs	1.06049 V	1.05069 V
$\Delta V_{th,predict}$ at 300 μs	9.80 mV	
$\Delta V_{th,actual}$	10.00 mV	

V_{th} is measured during the display turn-off state, and V_{th} shift is tracked in the display turn-on state.

III. SIMULATION AND RESULT

We simulated the proposed compensation method using Smart SPICE. We developed the SPICE model library based on the central data of measured oxide TFTs, as shown in Fig. 5. After that, we used Monte-Carlo simulation to make random parameter sets. Our method can predict the V_{th} shift in a short time even though TFTs suffer from mobility variation. Thus, mobility variation was reproduced in

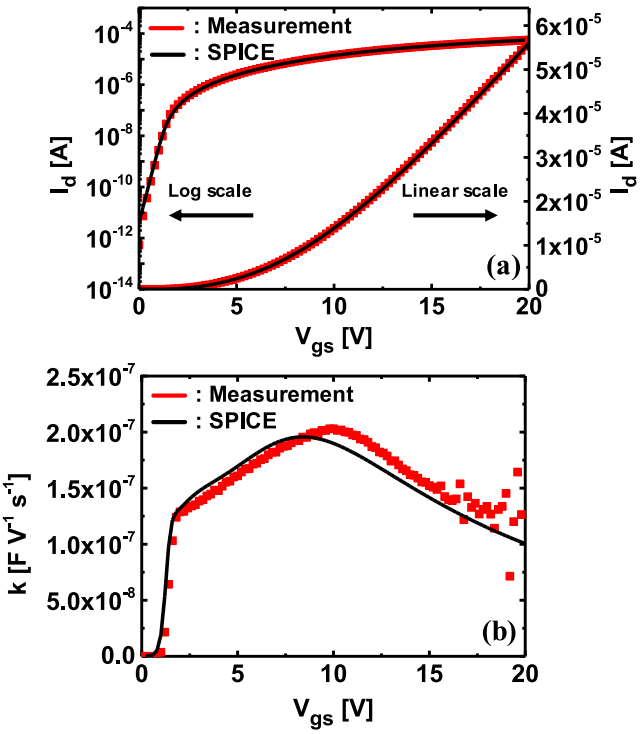

FIGURE 5. (a) Transfer curve of SPICE oxide TFT model and measurement data. (b) k-V_{gs} curve extracted from the transfer curve of SPICE oxide TFT model and measurement data.

the simulation. We gave variations to the SPICE parameters MU0, MU1, and MUS, which are related to high field mobility, low field mobility, and subthreshold mobility, respectively. We set parameters to make 10k TFTs following Gaussian distribution with the mean values of 0.7 V and 7.7 cm^2/V·s and the three standard deviations of 2.3 cm^2/V·s The mean values represent the conventional oxide TFT performances [21]–[23]. Due to the parameter variation, the maximum mobility can decrease by up to 30%. Then, we adjusted parameter VTO to represent V_{th} degradation.

Based on 10k TFTs' V_s-time curves, we verified the accuracy of the proposed method. The prediction error was calculated from the difference between the predicted ΔV_{th} and the actual ΔV_{th}. We calculated V_{th} before and after the degradation using the proposed method, when t_p is 100, 200, and 300 μs and Δt is 10 μs. Δt can be a value other than 10 us. When Δt is increased, the ADC's resolution in the driver ICs can be decreased. Then, ΔV_{th} was obtained.

Considering 4K UHD (3840×2160) resolution display with 120 Hz refresh rate, vertical blank time is approximately 500 μs with 140 vertical dummy lines. For a 120 Hz refresh rate, V_{th} degradation of one horizontal line can be calculated every 1/120 seconds. When RGB sub-pixels share one sensing bus line, each sub-pixel can be compensated every 54 seconds (1/120×2160×3). When TFT suffers from positive bias temperature stress (PBTS) conditions for 54 seconds, V_{th} shift of oxide TFT is about 100 mV [24]–[26]. However, TFT in the real display panel would be exposed to

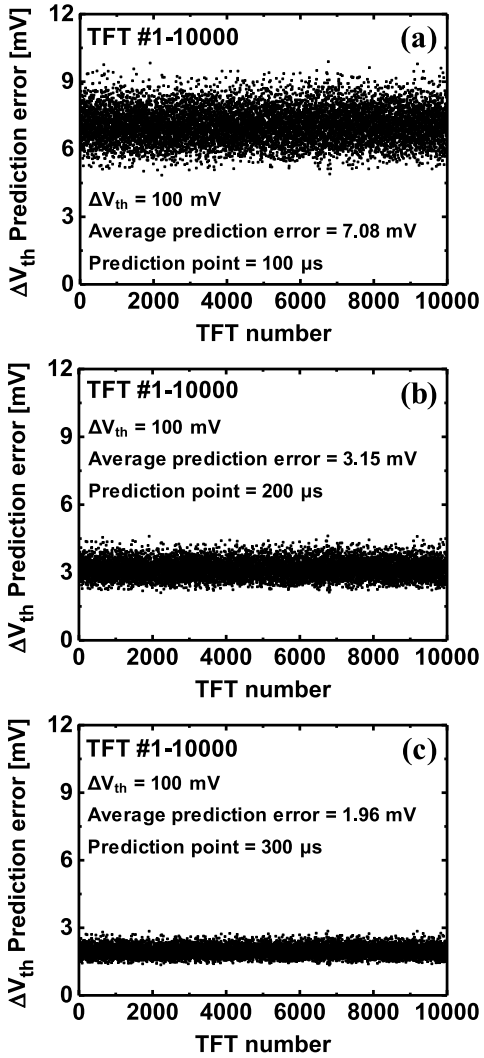

FIGURE 6. (a) Prediction errors of 10000 random TFTs when ΔV_{th} is 100 mV and the predict point is 100 μs (b) 200 μs, and (c) 300 μs.

TABLE 2. Acceptable prediction error at low, middle, and high gray level.

	Acceptable prediction error
Low gray level	3.8 mV
Middle gray level	5.4 mV
High gray level	8.9 mV

a smaller stress condition than PBTS. Thus, the maximum V_{th} shift of oxide TFT will be within 100 mV during one cycle. Therefore, t_p up to 300 μs, and V_{th} shift of 100 mV are quite marginal and reasonable experiments.

Fig. 6 shows the result of each case. We found out that the distribution and average of prediction errors decreased as the prediction point increased. In the case of 300 μs, almost all of the prediction errors are within 3 mV, and the average error is also very small, about 2 mV.

Meanwhile, we considered the just noticeable difference (JND) to set the acceptable prediction error. The JND is the threshold of change that the human visual system (HVS) can perceive. If the adaptation luminance is L and JND is ΔL, the HVS cannot perceive foreground stimulus of luminance between $L-\Delta L$ and $L+\Delta L$. To calculate the acceptable ΔL and corresponding prediction error, the grayscale standard display function [27] is used.

First, a 2.2 gamma curve is generated for the grayscale indexes from 0 to 255, where the maximum luminance is assumed to be 150 nits. After that, the luminance at 30, 128, and 255 grayscale indexes are extracted for the analysis at the low, middle, and high gray levels. Then, JND index of each luminance is calculated from the grayscale standard display function. Because the HVS can perceive the change between L(JND index) and L(JND index+1), ΔL should be smaller than the difference between this two luminance. Here, L(JND index+1) is calculated from the inverse function [27]. After that, the equation $\mathrm{I} = A\cdot(L/\alpha)$, is used to calculate the OLED current required for L(JND index) and L(JND index+1). In the equation, L is the luminance, α is the current efficiency, and A is the luminous area. In this article, DuPont's blue OLED current efficiency $\alpha = 5.3$ cd/A [28], and 55 inch 4K UHD TV's pixel size $A = (1.21\ \mathrm{m}\times 0.68\ \mathrm{m})/(3840\times 2160\times 3) = 3.307\times 10^{-8}\ \mathrm{m}^2$ is used. Finally, we can get the acceptable prediction error from the difference between the V_{gs} required for each calculated OLED current. The acceptable errors are shown in Table 2. From Table 2, it can be said that the proposed method can be used in low gray level compensation if the prediction point is 300 μs.

IV. CONCLUSION

In this article, we proposed a novel real-time V_{th} compensation method. The proposed method predicts the V_{th} degradation based on a prediction equation, which is derived from C_{line} charging with I_d of T 1. The V_{th} degradation can be predicted even under the mobility variation, since V_{gs} dependence of k is considered with consecutive source node voltage detection. Since the proposed method only takes hundreds of microseconds, the real-time V_{th} shift prediction can be carried out during a vertical blank time of 4K UHD resolution display. Also, Smart SPICE simulation with severe mobility variation showed that the prediction error was within one JND margin though out all gray levels. Therefore, the proposed method is promising for the high resolution, large-sized and sustainable OLED display.

APPENDIX A
DERIVATION OF (6)

The equation (6) is derived as follows. The equation (5) is transformed into

$$V_g - V_s(t) - V_{th} = \frac{1}{\frac{1}{V_g - V_s(0) - V_{th}} + \frac{k}{C_{line}}t}. \qquad \text{(A1)}$$

Then, (A1) can be expressed as

$$\frac{1}{A} - \gamma = \frac{1}{A+\beta}\ , \tag{A2}$$

where

$$A = \frac{1}{V_g - V_s(0) - V_{th}}, \tag{A3}$$

$$\beta = \frac{k}{C_{line}}t, \tag{A4}$$

$$\gamma = V_s(t) - V_s(0). \tag{A5}$$

In the quadratic equation form, (A2) is expressed as

$$(1-\gamma A)(A+\beta) = A. \tag{A6}$$

By applying quadratic formula to (A6),

$$A = \frac{-\beta\gamma + \sqrt{\beta^2\gamma^2 + 4\beta\gamma}}{2\gamma}, \tag{A7}$$

is obtained, since A>0. From (A3) and (A7),

$$V_g - V_s(0) - V_{th} = \frac{2\gamma}{-\beta\gamma + \sqrt{\beta^2\gamma^2 + 4\beta\gamma}} \tag{A8}$$

is obtained. The equation (6) is mathematically equal to (A8).

APPENDIX B
DERIVATION OF (9)

The equation (9) is derived as follows. The equation (3) is transformed into

$$I_d = C_{line} \times \frac{dV_s(t)}{dt}. \tag{B1}$$

By considering the time-varying voltage dependence of k, (B1) is expressed as

$$k(t) \times [V_g - V_s(t) - V_{th}]^2 = C_{line} \times \frac{dV_s(t)}{dt}. \tag{B2}$$

Since dt and $dV_s(t)$ can be assumed as Δt and $\Delta V_s(t)$ for a short time, (B2) is expressed as

$$k(t) \times [V_g - V_s(t) - V_{th}]^2 \times \Delta t = C_{line} \times \Delta V_s(t). \tag{B3}$$

By substituting $\Delta V_s(t)$ *to* $V_s(t+\Delta t) - V_s(t)$, (B3) is expressed as

$$k(t) = \frac{C_{line} \times [V_s(t+\Delta t) - V_s(t)]}{\left[V_g - V_s(t) - V_{th}\right]^2 \times \Delta t}. \tag{B4}$$

The equation (9) is equal to (B4).

APPENDIX C
DERIVATION OF (13)

The equation (13) is derived as follows. When $V_s(0)$ =0 V, the equation (6) is simplified as

$$V_g - V_{th} = \frac{2\gamma}{-\beta\gamma + \sqrt{\beta^2\gamma^2 + 4\beta\gamma}}, \tag{C1}$$

$$\beta = \frac{k}{C_{line}}t, \tag{C2}$$

$$\gamma = V_s(t). \tag{C3}$$

By multiplying the denominator and numerator on the right side of (C1) by $(1/\gamma)(\beta + \sqrt{\beta^2 + 4\beta/\gamma})$,

$$\frac{2\gamma}{-\beta\gamma + \sqrt{\beta^2\gamma^2 + 4\beta\gamma}} \times \frac{\frac{1}{\gamma}}{\frac{1}{\gamma}} = \frac{2}{-\beta + \sqrt{\beta^2 + \frac{4\beta}{\gamma}}}, \tag{C4}$$

$$\frac{2}{-\beta + \sqrt{\beta^2 + \frac{4\beta}{\gamma}}} \times \frac{\beta + \sqrt{\beta^2 + \frac{4\beta}{\gamma}}}{\beta + \sqrt{\beta^2 + \frac{4\beta}{\gamma}}} = \frac{2}{\frac{4\beta}{\gamma}}\left(\beta + \sqrt{\beta^2 + \frac{4\beta}{\gamma}}\right) = \frac{\gamma}{2} + \sqrt{\frac{\gamma^2}{4} + \frac{\gamma}{\beta}} \tag{C5}$$

is obtained. Then, (C1) is expressed as

$$V_g - V_{th} = \frac{V_s(t)}{2} + \sqrt{\frac{V_s(t)^2}{4} + \frac{V_s(t)}{\beta}}, \tag{C6}$$

by (C3) and (C5). By subtracting $V_s(t)/2$ from both sides of (C6) and squaring them, (C6) is expressed as

$$\left[V_g - V_{th} - \frac{V_s(t)}{2}\right]^2 = \frac{V_s(t)^2}{4} + \frac{V_s(t)}{\beta}. \tag{C7}$$

From (C7),

$$\left(V_g - V_{th}\right)^2 - V_s(t)\left(V_g - V_{th}\right) = \frac{V_s(t)}{\beta} \tag{C8}$$

is obtained. By considering the time-varying voltage dependence of k, β is expressed as

$$\beta = \frac{[V_s(t+\Delta t) - V_s(t)]t}{\Delta t\left[V_g - V_s(t) - V_{th}\right]^2} \tag{C9}$$

by (9) and (C2). The equation (12) is obtained by substituting β as (C9) in (C8). Then, the equation (12) can be expressed as

$$B^2 - V_s(t)B = \frac{V_s(t)}{\frac{[V_s(t+\Delta t) - V_s(t)]t}{\Delta t[B - V_s(t)]^2}} = \frac{V_s(t)\Delta t}{[V_s(t+\Delta t) - V_s(t)]t}[B - V_s(t)]^2 \tag{C10}$$

where

$$B = V_g - V_{th}. \tag{C11}$$

By dividing both sides of (C10) by $[B - V_s(t)]$,

$$B = \frac{V_s(t)\Delta t}{[V_s(t+\Delta t) - V_s(t)]t}[B - V_s(t)] \tag{C12}$$

is obtained. From (C11) and (C12),

$$V_g - V_{th} = \frac{\frac{V_s(t)^2 \Delta t}{[V_s(t+\Delta t) - V_s(t)]t}}{\frac{V_s(t)\Delta t}{[V_s(t+\Delta t) - V_s(t)]t} - 1} \tag{C13}$$

is obtained. The equation (13) is equal to (C13).

REFERENCES

[1] C. W. Tang and S. A. VanSlyke, "Organic electroluminescent diodes," *Appl. Phys. Lett.*, vol. 51, no. 12, pp. 913–915, 1987.
[2] M. A. Baldo *et al.*, "Highly efficient phosphorescent emission from organic electroluminescent devices," *Nature*, vol. 395, no. 6698, pp. 151–154, 1998.
[3] M. Stewart, R. S. Howell, L. Pires, and M. K. Hatalis, "Polysilicon TFT technology for active matrix OLED displays," *IEEE Trans. Electron Devices*, vol. 48, no. 5, pp. 845–851, May 2001.
[4] Y. He, R. Hattori, and J. Kanicki, "Current-source a-Si: H thin-film transistor circuit for active-matrix organic light-emitting displays," *IEEE Electron Device Lett.*, vol. 21, no. 12, pp. 590–592, Dec. 2000.
[5] B. Geffroy, P. le Roy, and C. Prat, "Organic light-emitting diode (OLED) technology: Materials, devices and display technologies," *Polym. Int.*, vol. 55, no. 6, pp. 572–582, Jun. 2006.
[6] S. Takasugi *et al.*, "Advanced compensation technologies for large-sized UHD OLED TVs," *J. Soc. Inf. Display*, vol. 24, no. 7, pp. 410–418, 2016.
[7] G. R. Chaji *et al.*, "Electrical compensation of OLED luminance degradation," *IEEE Electron Device Lett.*, vol. 28, no. 12, pp. 1108–1110, Dec. 2007.
[8] G. R. Chaji *et al.*, "Stable RGBW AMOLED display with OLED degradation compensation using electrical feedback," in *Proc. IEEE Int. Solid-State Circuits Conf. (ISSCC)*, 2010, pp. 118–119.
[9] K. Inukai *et al.*, "36.4L: Late-news paper: 4.0-in. TFT-OLED displays and a novel digital driving method," in *SID Symp. Dig.*, vol. 31, 2000, pp. 924–927.
[10] H.-J. In and O.-K. Kwon, "External compensation of nonuniform electrical characteristics of thin-film transistors and degradation of OLED devices in AMOLED displays," *IEEE Electron Device Lett.*, vol. 30, no. 4, pp. 377–379, Apr. 2009.
[11] T. Sasaoka *et al.*, "24.4L: Late-news paper: A 13.0-inch AM-OLED display with top emitting structure and adaptive current mode programmed pixel circuit (TAC)," in *SID Symp. Dig.*, vol. 32, 2001, pp. 384–387.
[12] K.-Y. Lee and P. C.-P. Chao, "A new AMOLED pixel circuit with pulsed drive and reverse bias to alleviate OLED degradation," *IEEE Trans. Electron Devices*, vol. 59, no. 4, pp. 1123–1130, Apr. 2012.
[13] J. Fu *et al.*, "16-3: A fast TFT threshold voltage sensing method based on iterative feedback," in *SID Symp. Dig.*, vol. 48, 2017, pp. 204–206.
[14] T. Hasumi, S. Takasugi, K. Kanoh, and Y. Kobayashi, "46.2: New OLED pixel circuit and driving method to suppress threshold voltage shift of a-Si: H TFT," in *SID Symp. Dig. Tech. Papers*, vol. 37, 2006, pp. 1547–1550.
[15] Y. H. Jang *et al.*, "7-4: Invited paper: Internal compensation type oled display using high mobility oxide tft," in *SID Symp. Dig. Tech. Papers*, vol. 48, 2017, pp. 76–79.
[16] H.-J. Shin *et al.*, "50.1: Invited paper: Technological progress of panel design and compensation methods for large-size UHD OLED TVs," in *SID Symp. Dig. Tech. Papers*, vol. 45, 2014, pp. 720–723.
[17] H. J. Shin *et al.*, "7.1: Invited paper: Novel oled display technologies for large-size UHD OLED TVs," in *SID Symp. Dig. Tech. Papers*, vol. 46, 2015, pp. 53–56.
[18] Y.-F. Jin and H.-J. Xie, "P-1.8: External compensation for TFT Vth&mobility using linear charge sense method in AMOLED display," in *SID Symp. Dig.*, vol. 49, Apr. 2018, pp. 541–543.
[19] U.-G. Min and O.-K. Kwon, "Real-time external sensing and compensation method for organic light emitting diode displays," *Electron. Lett.*, vol. 45, no. 24, pp. 1232–1234, 2009.
[20] R. Tani *et al.*, "64.2: Panel and circuit designs for the world's first 65-inch UHD OLED TV," in *SID Symp. Dig. Tech. Papers*, vol. 46, 2015, pp. 950–953.
[21] J. F. Wager, "Oxide TFTs: A progress report," *Inf. Display Arch.*, vol. 32, no. 1, pp. 16–21, 2016.
[22] J. Y. Noh, D. M. Han, W. C. Jeong, J. W. Kim, and S. Y. Cha, "Development of 55" 4K UHD OLED TV employing the internal gate IC with high reliability and short channel IGZO TFTs," *J. Soc. Inf. Display*, vol. 26, no.1, pp. 36–41, 2018.
[23] Y.-M. Ha, S. K. Kim, H. Choi, S.-G. Lee, K.-S. Park, and I. Kang, "69-1: Invited Paper: Oxide TFT development for AMLCDs and AMOLEDs," in *SID Symp. Dig. Tech. Papers*, vol. 47, 2016, pp. 940–943.
[24] K.-S. Park, S. Oh, P. Yun, J. Uk Bae, and I. B. Kang, "Prospects of oxide TFTs approaching LTPS," in *Proc. Int. Workshop Active-Matrix Flatpanel Displays Devices (AM-FPD)*, 2015, pp. 241–244.
[25] H. Yamaguchi *et al.*, "74.2 L: Late-News Paper: 11.7-inch flexible AMOLED display driven by a-IGZO TFTs on plastic substrate," in *SID Symp. Dig. Tech. Papers*, vol. 43, 2012, pp. 1002–1005.
[26] Y. G. Mo *et al.*, "Amorphous-oxide TFT backplane for large-sized AMOLED TVs," *J. Soc. Inf. Display*, vol. 19, no. 1, pp. 16–20, 2011.
[27] *Digital Imaging and Communications in Medicine (DICOM) Part 14: Grayscale Standard Display Function*. Arlington, VA, USA: Nat. Electr. Manuf. Assoc., 2006.
[28] R. J. Chesterfeild *et al.*, "38-3: Invited paper: Solution printing for OLED televisions," in *SID Symp. Dig.*, vol. 47, 2016, pp. 491–493.